Supporting information

Furanmonogones A and B: two rearranged acylphloroglucinols with a 4,5-*seco*-3(2H)-furanone core from the flowers of *Hypericum monogynum*

Wen-Jun Xu,[1] Jun Luo,[1] Rui-Jun Li, Ming-Hua Yang, and Ling-Yi Kong*

State Key Laboratory of Natural Medicines, Department of Natural Medicinal Chemistry, China Pharmaceutical University, 24 Tong Jia Xiang, Nanjing 210009, People's Republic of China

* Corresponding author:
Tel/Fax: +86-25-83271405
E-mail: cpu_lykong@126.com;

Table of Contents Page

Experimental Section

Computational Data

NMR, HRESIMS, IR, UV, and ECD Spectra of Compounds 1 and 2.

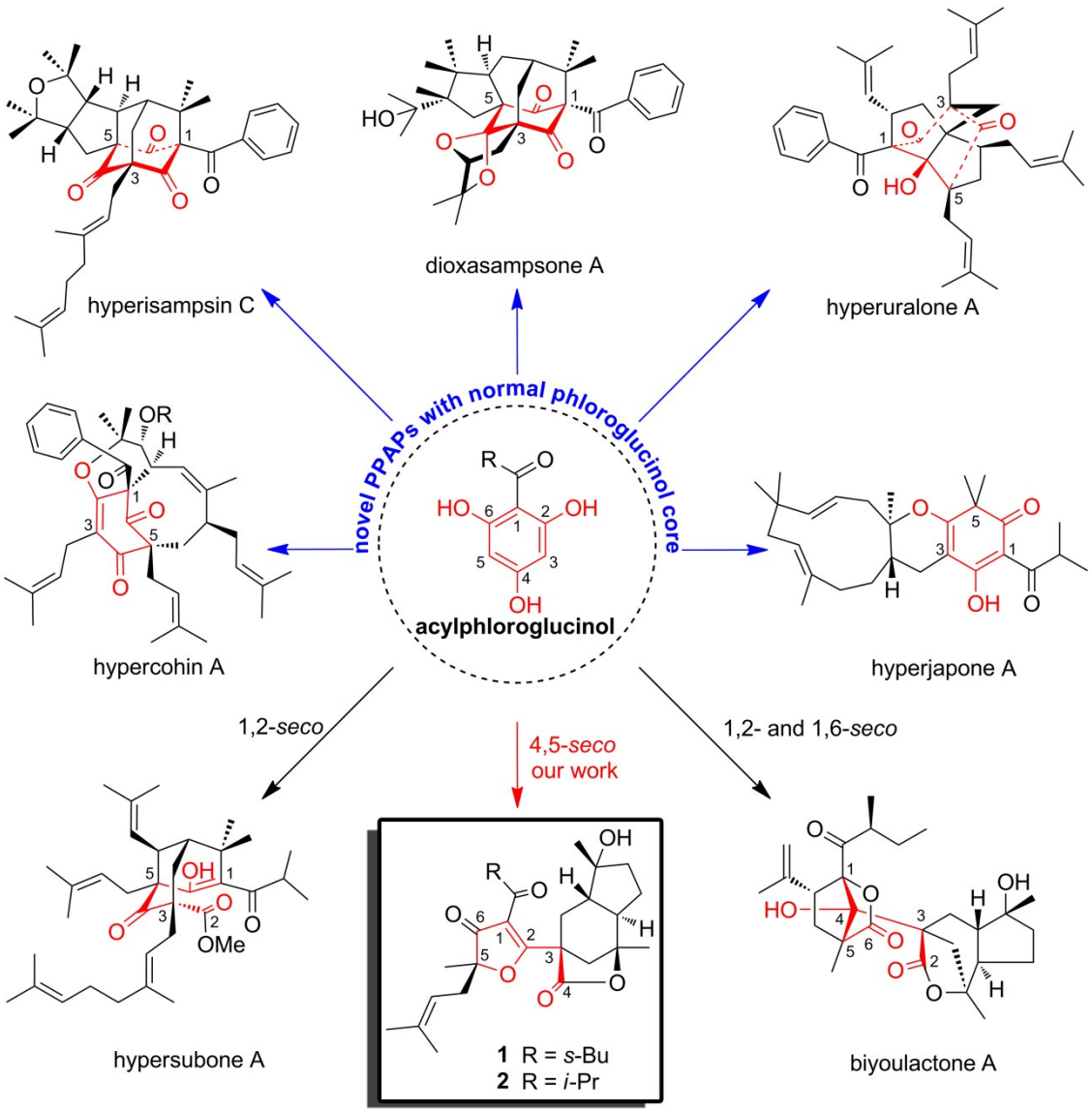

Figure S1. Novel PPAPs scaffolds originated from acylphloroglucinol.[1]

Experimental Sections

General Experiment Procedures

Optical rotations were measured on a JASCO P-1020 polarimeter. The UV spectra were recorded on a UV-2450 UV/vis spectrophotometer. The ECD spectra were recorded on a JASCO J-810 spectrometer. The IR measurements were performed on a Bruker Tensor 27 spectrometer. The ^{1}H, ^{13}C, HSQC, HMBC and ROESY NMR spectra were recorded on a Bruker Avance III NMR spectrometer using standard pulse sequences (^{1}H: 500 MHz, ^{13}C: 125 MHz) with TMS as an internal standard in $CDCl_3$. The HRESIMS spectra were acquired using an Agilent 6520B UPLC-Q-TOF mass spectrometer. Column chromatography was carried out using silica gel (100-200

mesh and 200-300 mesh; Qingdao Haiyang Chemical Co., Ltd., Qingdao, China), Sephadex LH-20 (40-70 μm; Amersham Pharmacia Biotech AB, Uppsala, Sweden), and ODS RP-C_{18} (40-63 μm, Fuji, Japan). Fractions obtained from column chromatography were monitored by TLC on precoated silica gel GF_{254} plates (Qingdao Haiyang Chemical Co. Ltd., Qingdao, China). The spots were visualized under UV light and by spraying the plates with a 1% vanillin-H_2SO_4 solution, followed by heating. The instrument used for HPLC analysis was an Agilent 1100 series chromatograph equipped with a DAD detector and an Agilent ZORBAX Eclipse XDB-C_{18} (5 μm, 4.6 × 150 mm^2, i.d.) column. Preparative HPLC was carried out using a SHIMADZU LC-6AD series instrument equipped with a Shim-pack RP-C_{18} column (10 μm, 20 × 200 mm^2, i.d.) and a binary-channel UV detector set to detect at 254 and 280 nm.

Plant Material

The fresh flowers of *H. monogynum* were collected from China Pharmaceutical University (Nanjing, Jiangsu Province, People's Republic of China) in June 2012. The plant material was authenticated by Professor Min-Jian Qin (China Pharmaceutical University). A voucher specimen (No. 2012-HML) was deposited at the Department of Natural Medicinal Chemistry, China Pharmaceutical University.

Extraction and Isolation

The fresh flowers of *H. monogynum* (7.0 kg) were extracted with 95% aqueous EtOH (3 × 10.0 L) under ultrasonic agitation at 90 Hz and 40 °C. After the solvent was removed under reduced pressure, the crude extract (202.5 g) was suspended in H_2O (1.0 L) and partitioned into petroleum ether (3 × 2.0 L). The petroleum ether extract (43.1 g) was loaded onto a silica gel column (100-200 mesh; 500.0 g; ⌀ 15.0 × 30.0 cm^2) and eluted with a gradient of petroleum ether-acetone (100:1 to 1:1, v/v) to give seven fractions (A-G). Fraction D (14.0 g) was separated on a silica gel column (200-300 mesh; 300.0 g; ⌀ 6.0 × 40.0 cm^2) eluting with petroleum ether/EtOAc (50:1 to 1:1, v/v) to give five major subfractions (Fr. DA-DE). Fraction DD (2.5 g) was

separated on a ODS RP-C_{18} column (40-63 μm; 100.0 g; ⌀ 3.0 × 45.0 cm^2) (MeOH/H_2O, 45:65 to 90:10, v/v) to give six subfractions (Fr. DD1-DD2). Fraction DD1 (256.1 mg) was chromatographed on Sephadex LH-20 (MeOH) and was further purified by preparative HPLC to afford compounds **1** (4 mg) and **2** (6 mg) using 62% MeOH in H_2O. Compounds **3** (930 mg) and **4** (580 mg) were purified from fraction B (8.3 g) on an ODS RP-C_{18} column using 80% MeOH in H_2O.

Physical and Spectroscopic Data of Compounds 1 and 2

*Furanmonogone A (**1**):* red oil; $[\alpha]^{25}_{D}$ −12 (*c* 0.1, MeOH); UV (MeOH) λ_{max} (log ε) 203 (3.79), 231 (3.80), 279 (3.81) nm; IR (KBr) ν_{max} 3444, 2965, 2923, 1780, 1761, 1704, 1671, 1539, 1454, 1398, 1383, 948, 915, 858 cm^{-1}; ECD (MeOH) λ ($\Delta\varepsilon$) 200 (+10.46), 219 (+7.58), 245 (−2.21), 277 (−4.22), 333 (−0.88), 366 (−2.46) nm; ^{1}H and ^{13}C NMR data, see Table 1 (Main Text); HRESIMS *m/z* 481.2565 $[M + Na]^+$ (calcd for $C_{27}H_{38}O_6Na$, 481.2561).

*Furanmonogone B (**2**):* red oil; $[\alpha]^{25}_{D}$ −8 (*c* 0.1, MeOH); UV (MeOH) λ_{max} (log ε) 203 (3.84), 231 (3.80), 277 (3.82) nm; IR (KBr) ν_{max} 3444, 2970, 2932, 1779, 1761, 1705, 1674, 1545, 1455, 1398, 996, 953, 916, 857 cm^{-1}; ECD (MeOH) λ ($\Delta\varepsilon$) 201 (+8.65), 218 (+6.77), 245 (−1.69), 277 (−3.86), 305 (−2.96), 328 (−0.94), 363 (−1.00) nm; ^{1}H and ^{13}C NMR data, see Table 1 (Main Text); HRESIMS *m/z* 467.2403 $[M + Na]^+$ (calcd for $C_{26}H_{36}O_6Na$, 467.2404).

NO Production Bioassay

The NO production was measured according to a published procedure.[2] *N*-Monomethyl-L-arginine was used as the positive control with IC_{50} values of 39.8 μM (in lipopolysaccharide-induced RAW264.7 cells model) and 39.3 μM (in lipopolysaccharide-induced BV-2 cells model). All experiments were performed in three independent replicates.

Computational Data

Quantum Chemical Prediction (QCP) of the ^{13}C NMR Data

QCP of the ^{13}C NMR chemical shift values were employed to solid the structure and the relative configurations of compound **1**. Based on the analyses of its 1D- and 2D-NMR data, the structure of **1** was depicted as shown in Figure S2-1 (**1A**). The other two candidates (**1B** and **1C**, Figure S2-1), which were deduced by analysis of the plausible biogenetic pathway of **1** (Scheme 1, Main Text), were also utilized for comparison.

Conformational analyses were initially performed using Confab[3] at MMFF94 force field for **1A**, **1B**, and **1C**. Room-temperature equilibrium populations were calculated according to Boltzmann distribution law (Equation 1). The conformers with Boltzmann-population over 1% were chosen for ^{13}C NMR calculations (Table S1).

$$\frac{N_i}{N} = \frac{g_i e^{-\frac{E_i}{k_B T}}}{\sum g_i e^{-\frac{E_i}{k_B T}}} \qquad \textbf{(1)}$$

Equation 1. N_i is the number of conformer i with energy E_i and degeneracy g_i at temperature T, and k_B is Boltzmann constant.

The theoretical calculations of each conformer were carried out using Gaussian 09.[4] First, the chosen conformers were optimized at B3LYP/6-31+G (d, p) in gas phase. The theoretical calculations of ^{13}C NMR data were conducted using the Gauge-Including Atomic Orbitals (GIAO) method at mPW1PW91/6-311+G (2d, p) in chloroform using the CPCM polarizable conductor calculation model. Finally, the ^{13}C NMR chemical shift values were averaged according to Boltzmann distribution for each conformer and empirically scaled with the experimental values (Table S2). Linear correlations between the calculated ^{13}C NMR chemical shifts acquired from QCP and the experimental shifts were also constructed (Figure S2-2).

The summary of regression analyses of theoretical and experimental ^{13}C NMR chemical shifts was shown in Table S3. There is an overall excellent agreement between theory and experiment ^{13}C NMR chemical shifts of structure **1A** with the corrected mean absolute deviation (CMAD) of 1.4 ppm and the corrected largest absolute deviation (CLAD) of 3.5 ppm, which further confirmed the structure and the relative configurations of compound **1**.

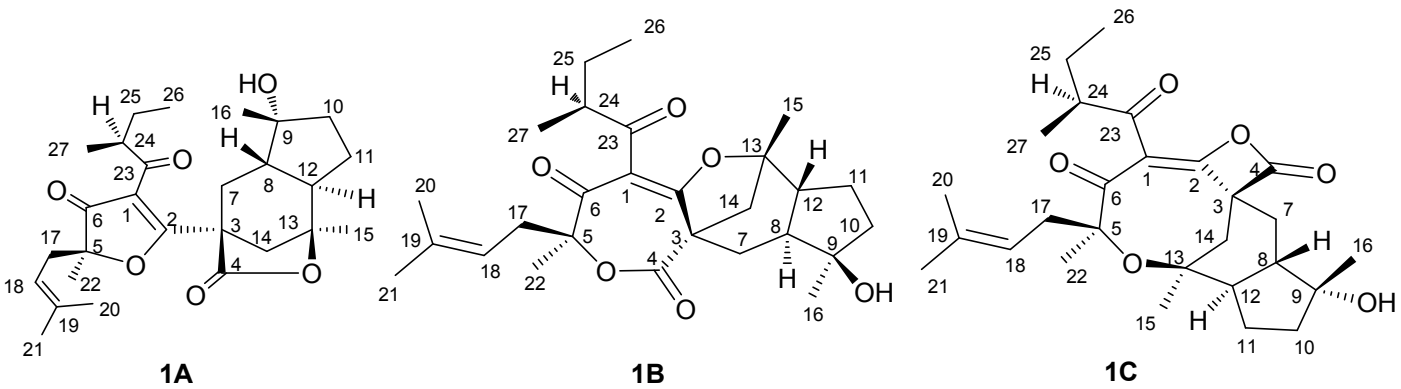

Figure S2-1. Structures of three candidates for ^{13}C NMR calculations.

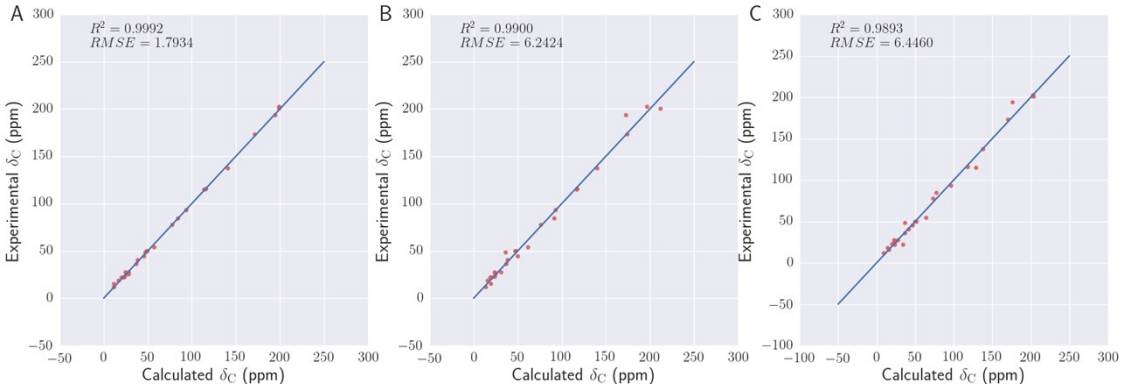

Figure S2-2. Linear correlations between the scaled calculated and experimental ^{13}C NMR chemical shifts for **1A** (A), **1B** (B), **and 1C** (C).

Table S1. Important thermodynamic parameters and Boltzmann distributions of the optimized conformers of **1A**, **1B**, and **1C** at B3LYP/6-31+G (d, p) level.

Isomer 1A					
Conformers	Structures	MMFF94	B3LYP/6-31+G (d, p)		
		E (kcal/mol)	E (Hartree)	E (kcal/mol)	Population (%)
1		102.96123	-1503.21840447	-943283.78	88.92
2	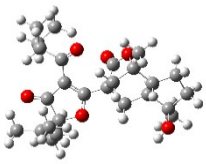	105.26697	-1503.22495388	-943287.89	1.81
3	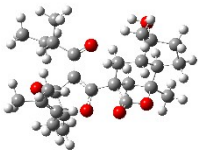	105.39380	-1503.21999031	-943284.78	1.46
4	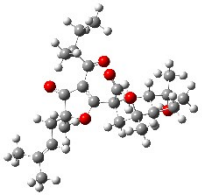	105.44982	-1503.21891348	-943284.10	1.33
5	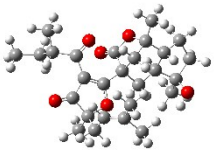	105.48628	-1503.22626317	-943288.71	1.25
Isomer 1B					
1	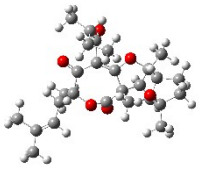	131.38837	-1503.17384333	-943255.82	97.38

Isomer 1C					
1	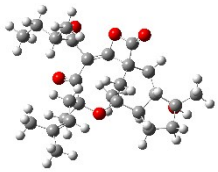	228.15754	-1658.98730984	-1041030.25	99.97

Table S2. Scaled Boltzmann averaged chemical shifts of isomer **1A**, scaled chemical shifts of **1B** and **1C**, and experimental chemical shifts.

Atom[a]	Experimental	**1A**	**1B**	**1C**
1	114.6	114.3	117.0	129.0
2	193.5	195.0	173.0	176.6
3	54.0	57.2	61.5	64.2
4	173.0	171.8	174.5	170.8
5	92.9	93.5	93.3	96.6
6	202.0	198.8	197.1	203.2
7	27.0	28.2	31.5	27.3
8	49.4	49.4	48.3	52.1
9	77.2	77.9	76.2	73.5
10	40.5	38.4	38.2	41.4
11	22.6	23.8	23.9	20.4
12	49.6	49.0	47.0	50.2
13	84.3	84.6	91.9	77.7
14	48.2	47.4	36.5	37.0
15	21.8	20.2	19.1	34.5
16	27.0	25.2	24.3	22.7
17	36.1	37.0	36.8	36.9
18	115.8	116.6	117.9	118.1
19	137.3	140.8	140.2	137.9
20	26.0	25.5	24.7	23.2
21	18.2	17.1	16.1	14.5

22	21.6	22.5	20.0	23.1
23	200.8	199.2	212.3	203.5
24	44.6	45.9	50.5	46.7
25	14.8	28.1	24.9	24.6
26	25.9	11.6	13.6	9.2
27	11.6	11.4	19.9	15.6
CMAD[b]		1.4	4.1	4.2
CLAD[c]		3.5	20.5	16.9

[a]see Figure S2-1.

[b]CMAD = corrected mean absolute deviation, computed as $(1/n)\sum_i^n |\delta_{comp} - \delta_{exp}|$ where δ_{comp} refers to the scaled computed chemical shifts.

[c]CLAD = corrected largest absolute deviation, computed as $\max(|\delta_{comp} - \delta_{exp}|)$.

Table S3. Summary of regression analyses of theoretical and experimental ^{13}C NMR chemical shifts.

Isomers	Conformers	CMAD	CLAD	R^2	Adjusted R^2	RMSE	F	p value
1A	1	1.7	4.7	0.9988	0.9987	2.2	20467.0	< 0.01
	2	1.4	3.8	0.9990	0.9990	1.9	26000.3	< 0.01
	3	1.2	4.5	0.9993	0.9992	1.7	34398.4	< 0.01
	4	2.0	8.1	0.9981	0.9981	2.7	13421.5	< 0.01
	5	1.4	4.0	0.9991	0.9991	1.8	29351.6	< 0.01
	Boltzmann	1.4	3.5	0.9992	0.9991	1.8	30285.0	< 0.01
1B	1	4.1	20.5	0.9900	0.9896	6.2	2476.8	< 0.01
1C	1	4.2	16.9	0.9893	0.9889	6.4	2321.3	< 0.01

ECD Spectra Calculation

The theoretical calculation of ECD was conducted using TDDFT method at B3LYP/6-311G** in methanol. Rotatory strengths for a total of 50 excited states were calculated. The ECD spectrum is simulated in SpecDis[5] by overlapping Gaussian

functions for each transition according to Equation 2:

$$\Delta\varepsilon(E) = \frac{1}{2.297\times10^{-39}} \times \frac{1}{\sqrt{2\pi\sigma}} \sum_{i}^{A} \Delta E_i R_i e^{-\left(\frac{E-E_i}{2\sigma}\right)^2} \quad \textbf{(2)}$$

Equation 2. σ represents the width of the band at 1/*e* height, and ΔE_i and R_i are the excitation energies and rotatory strengths for transition *i*, respectively.

ECD spectra of each configuration were weighted and summed up according to Boltzmann distribution, respectively. The absolute configurations of **1** were assigned as 3*S*, 5*S*, 8*S*, 9*R*, 12*R*, 13*S*, and 24*S* (Figure S2-3).

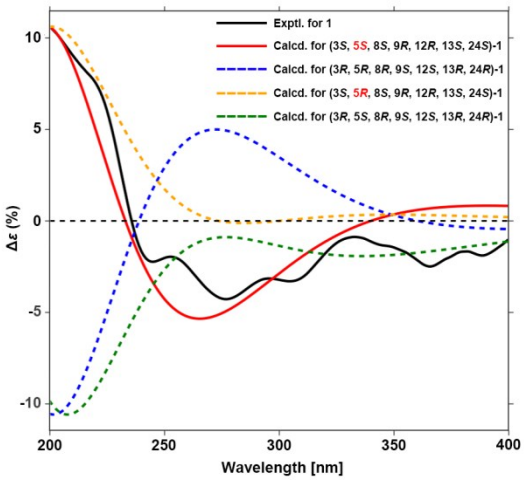

Figure S2-3. Experimental ECD spectrum of **1** and calculated ECD spectra of (3*S*, 5*S*, 8*S*, 9*R*, 12*R*, 13*S*, 24*S*)-**1** and (3*S*, 5*R*, 8*S*, 9*R*, 12*R*, 13*S*, 24*S*)-**1** and their enantiomers.

Reference

(1) (a) Yang, X. W.; Li, Y. P.; Su, J.; Ma, W. G.; Xu, G. *Org. Lett.* **2016**, *18*, 1876-1879. (b) Tian, W. J.; Qiu, Y. Q.; Yao, X. J.; Chen, H. F.; Dai, Y.; Zhang, X. K.; Yao, X. S. *Org. Lett.* **2014**, *16*, 6346-6349. (c) Zhu, H.; Chen, C.; Yang, J.; Li, X. N.; Liu, J.; Sun, B.; Huang, S. X.; Li, D.; Yao, G.; Luo, Z.; Li, Y.; Zhang, J.; Xue, Y.; Zhang, Y. H. *Org. Lett.* **2014**, *16*, 6322-6325. (d) Zhang, J. J.; Yang, J.; Liao, Y.; Yang, X. W.; Ma, J. Z.; Xiao, Q. L.; Yang, L. X.; Xu, G. *Org. Lett.* **2014**, *16*, 4912-4915. (e) Yang, X. W.; Deng, X.; Liu, X.; Wu, C. Y.; Li, X. N.; Wu, B.; Luo, H. R.; Li, Y.; Xu,

H. X.; Zhao, Q. S.; Xu, G. *Chem. Commun.* **2012**, *48*, 5998-6000. (f) Liao, Y.; Liu, X.; Yang, J.; Lao, Y. Z.; Yang, X. W.; Li, X. N.; Zhang, J. J.; Ding, Z. J.; Xu, H. X.; Xu, G. *Org. Lett.* **2015**, *17*, 1172-1175. (g) Tanaka, N.; Abe, S.; Hasegawa, K.; Shiro, M.; Kobayashi, J. *Org. Lett.* **2011**, *13*, 5488-5491.

(2) (a) Zhang, H. J.; Zhang, Y. M.; Luo, J. G.; Luo, J.; Kong, L. Y. *Org. Biomol. Chem.* **2015**, 13, 7452-7458. (b) Xu, W. J.; Li, R. J. Quasie, O.; Yang, M. H.; Kong, L. Y.; Luo, J. *J. Nat. Prod.* **2016**, 79, 1971-1981.

(3) Noel M OBoyle, Tim V, ermeersch, Christopher J Flynn, Anita R Maguire Maguire, and Geoffey R Hutchison. Confab - systematic generation of diverse low-energy conformers. *Journal of Cheminformatics*, 3:3–8, March 2011.

(4) M. J. Frisch, G. W. Trucks, H. B. Schlegel, G. E. Scuseria, M. A. Robb, J. R. Cheeseman, G. Scalmani, V. Barone, B. Mennucci, G. A. Petersson, H. Nakatsuji, M. Caricato, X. Li, H. P. Hratchian, A. F. Izmaylov, J. Bloino, G. Zheng, J. L. Sonnenberg, M. Hada, M. Ehara, K. Toyota, R. Fukuda, J. Hasegawa, M. Ishida, T. Nakajima, Y. Honda, O. Kitao, H. Nakai, T. Vreven, J. A. Montgomery, Jr., J. E. Peralta, F. Ogliaro, M. Bearpark, J. J. Heyd, E. Brothers, K. N. Kudin, V. N. Staroverov, R. Kobayashi, J. Normand, K. Raghavachari, A. Rendell, J. C. Burant, S. S. Iyengar, J. Tomasi, M. Cossi, N. Rega, J. M. Millam, M. Klene, J. E. Knox, J. B. Cross, V. Bakken, C. Adamo, J. Jaramillo, R. Gomperts, R. E. Stratmann, O. Yazyev, A. J. Austin, R. Cammi, C. Pomelli, J. W. Ochterski, R. L. Martin, K. Morokuma, V. G. Zakrzewski, G. A. Voth, P. Salvador, J. J. Dannenberg, S. Dapprich, A. D. Daniels, O. Farkas, J. B. Foresman, J. V. Ortiz, J. Cioslowski, and D. J. Fox. Gaussian 09 Revision D.01. Gaussian Inc. Wallingford CT 2009.

(5) Torsten Bruhn, Anu Schaumlffl, Anu Schaumlffl, Yasmin Hemberger, Yasmin Hemberger, Gerhard Bringmann, and Gerhard Bringmann. Specdis: quantifying the comparison of calculated and experimental electronic circular dichroism spectra. *Chirality*, 25(4):243–9, April 2013.

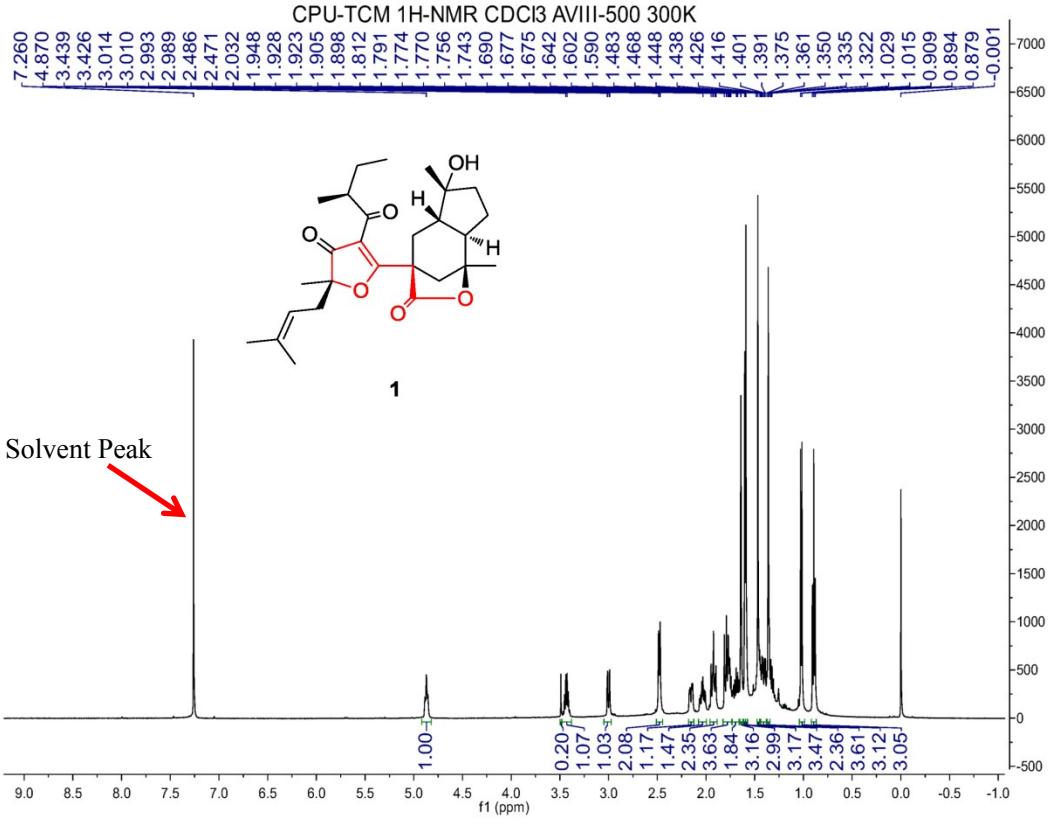

Figure S3-1. ^{1}H NMR spectrum of furanmonogone A (**1**) in $CDCl_3$

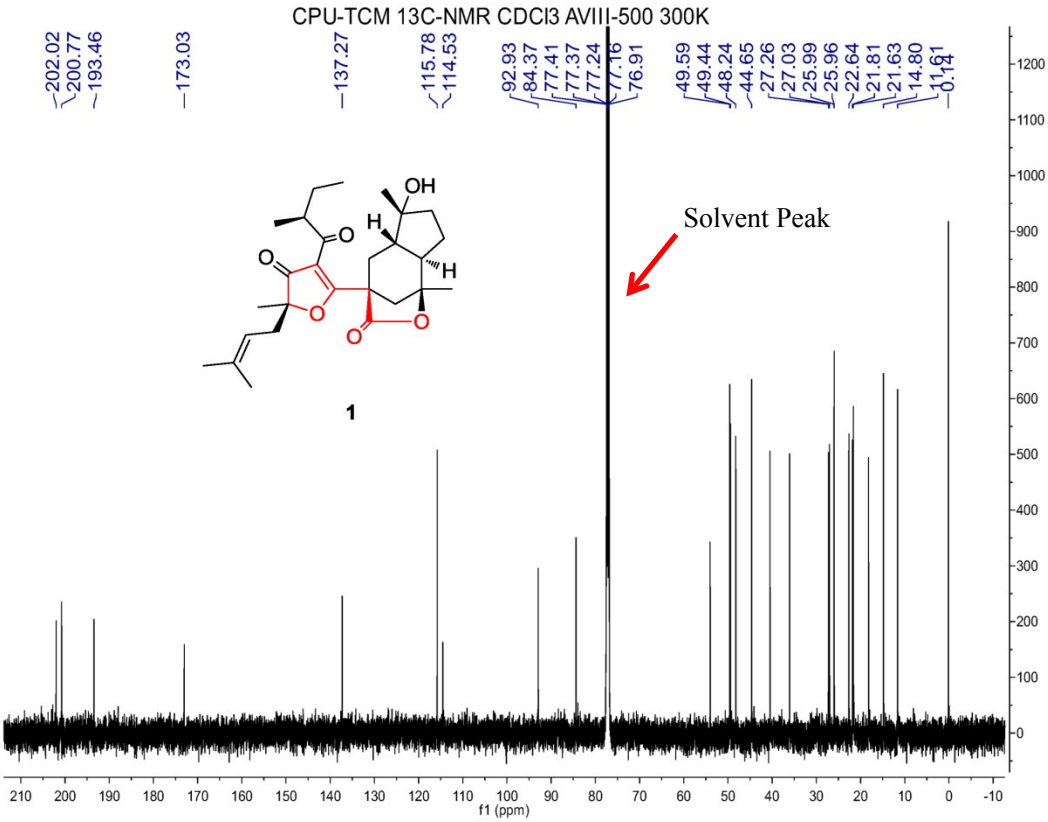

Figure S3-2. ^{13}C NMR spectrum of furanmonogone A (**1**) in $CDCl_3$

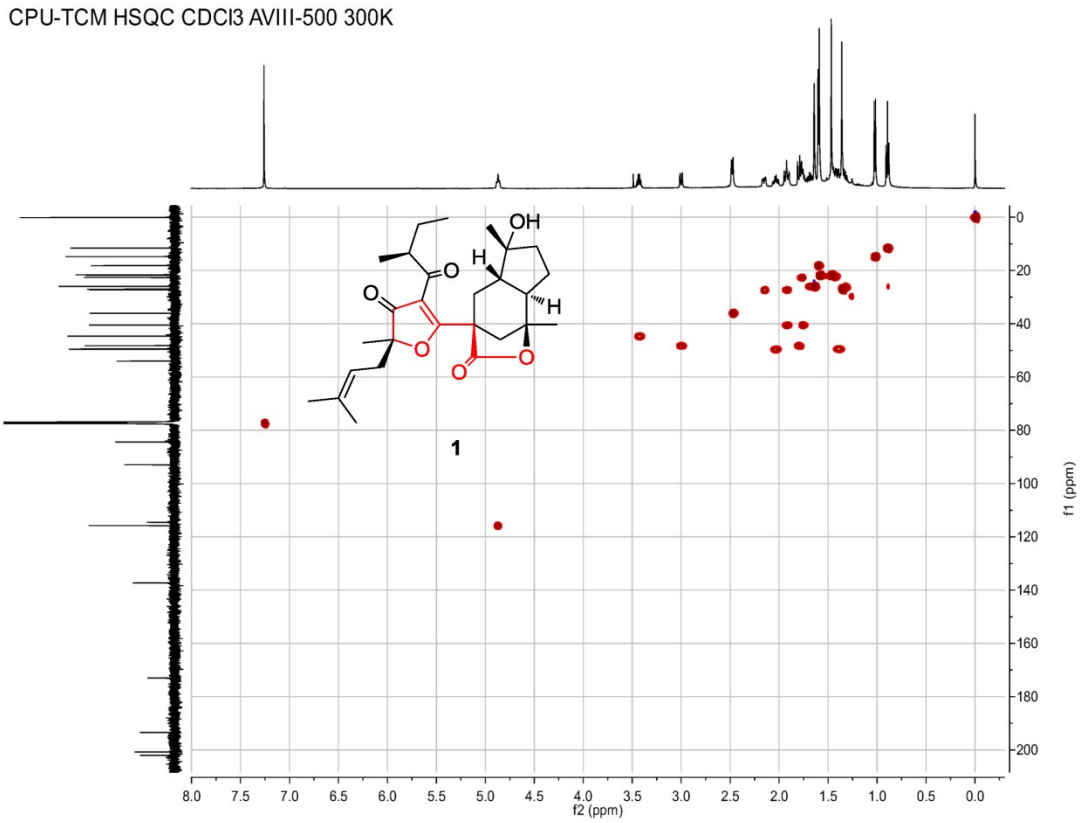

Figure S3-3. HSQC spectrum of furanmonogone A (**1**) in $CDCl_3$

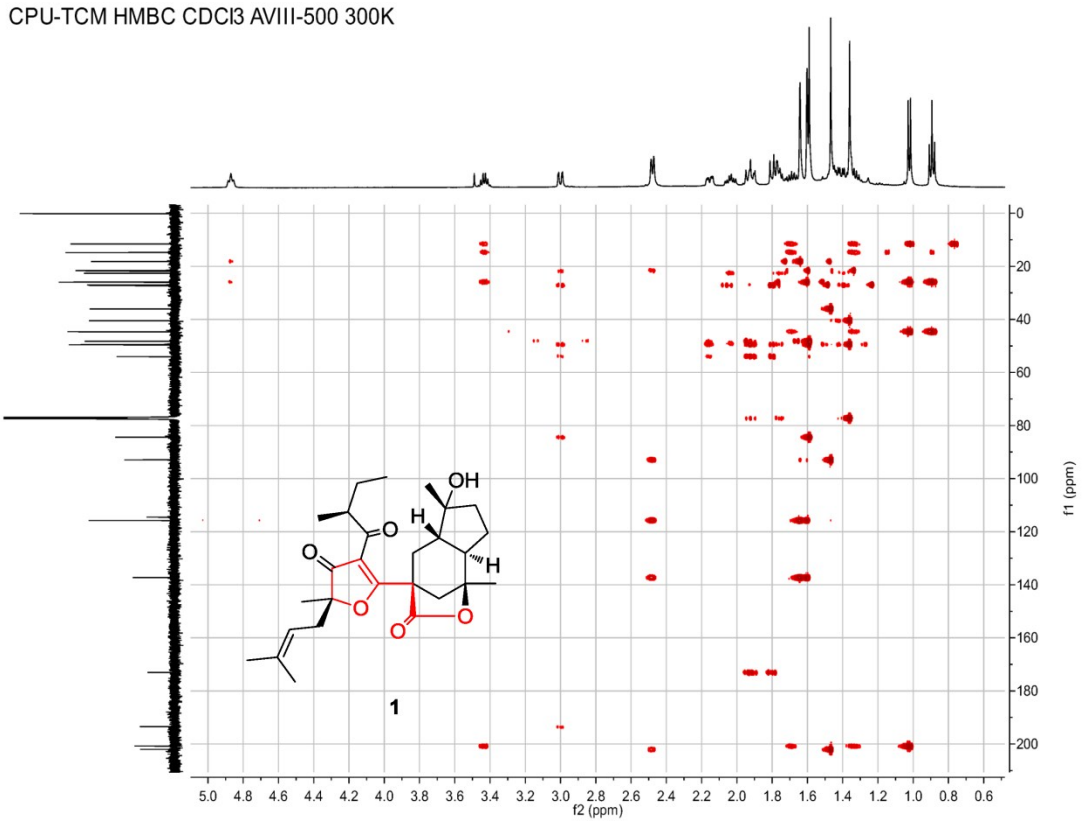

Figure S3-4. HMBC spectrum of furanmonogone A (**1**) in $CDCl_3$

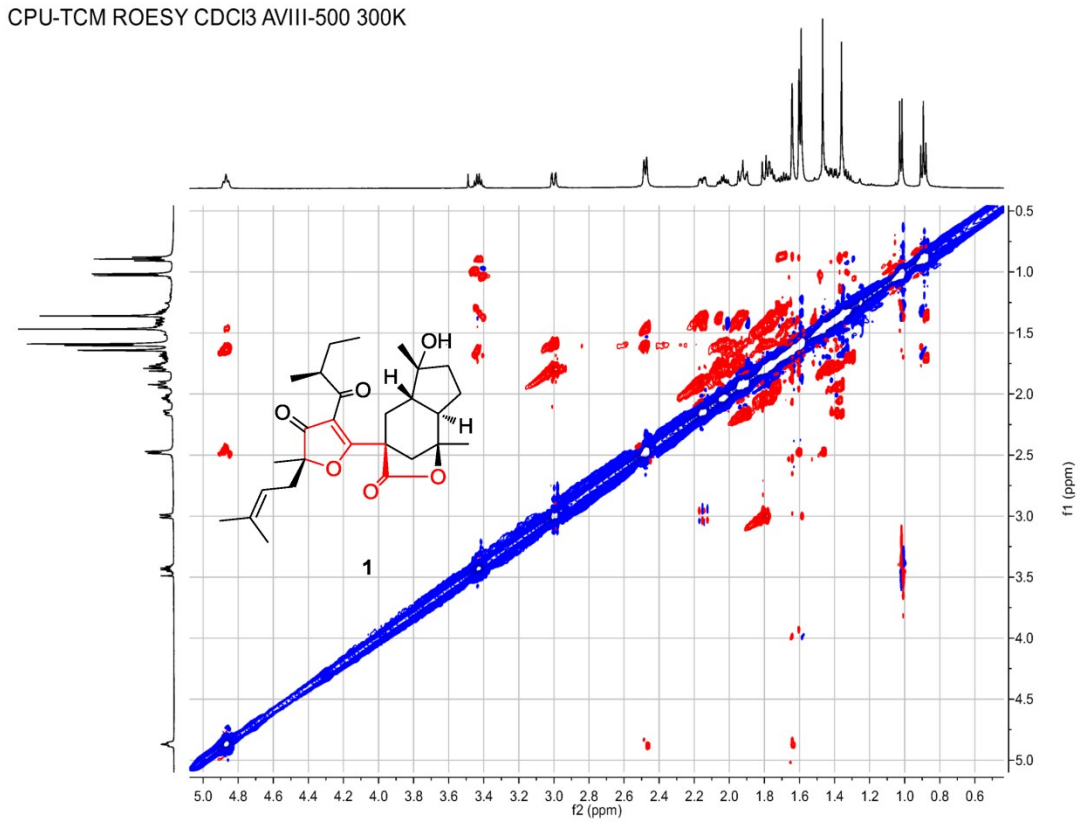

Figure S3-5. ROESY spectrum of furanmonogone A (**1**) in $CDCl_3$

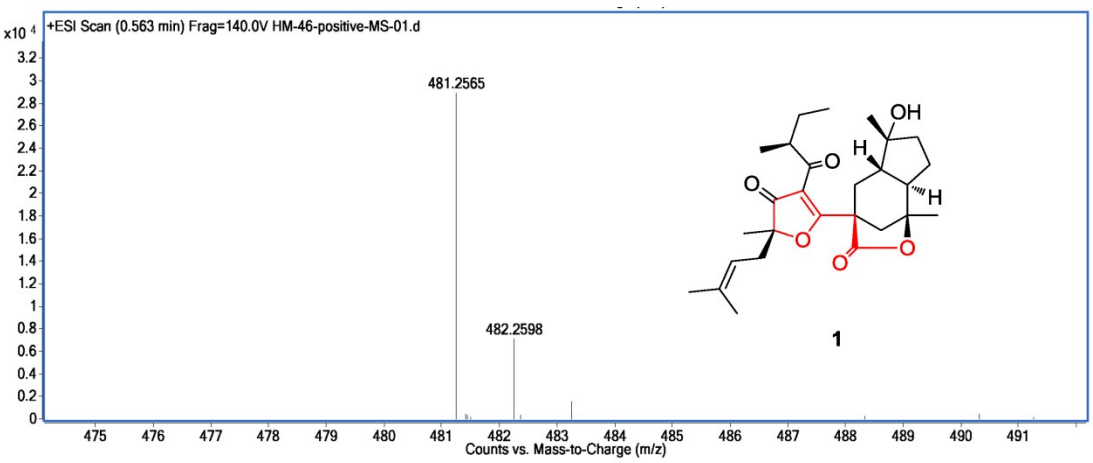

Elemental Composition Calculator

Target m/z:	481.2565	**Result type:**	Positive ions	**Species:**	$[M+Na]^+$
Elements:		C (0-80); H (0-120); O (0-30); N(0-10); Na (0-5); S (0-5)			
Ion Formula		**Calculated m/z**		**PPM Error**	
C27H38NaO6		481.2561		-0.86	

Figure S3-6. HRESIMS spectrum of furanmonogone A (**1**)

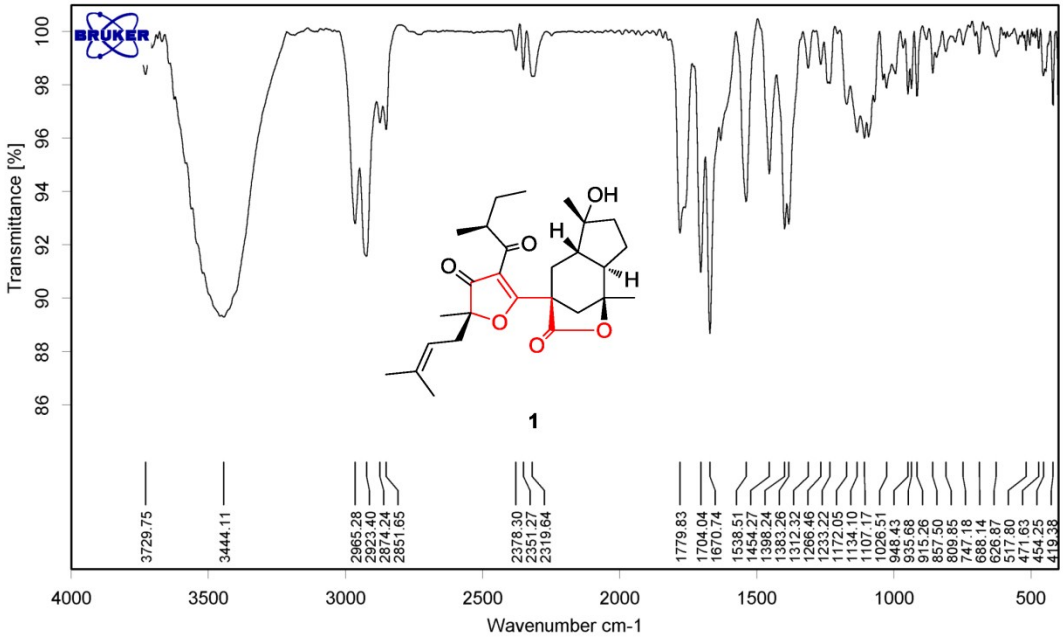

Figure S3-7. IR (KBr disc) spectrum of furanmonogone A (**1**)

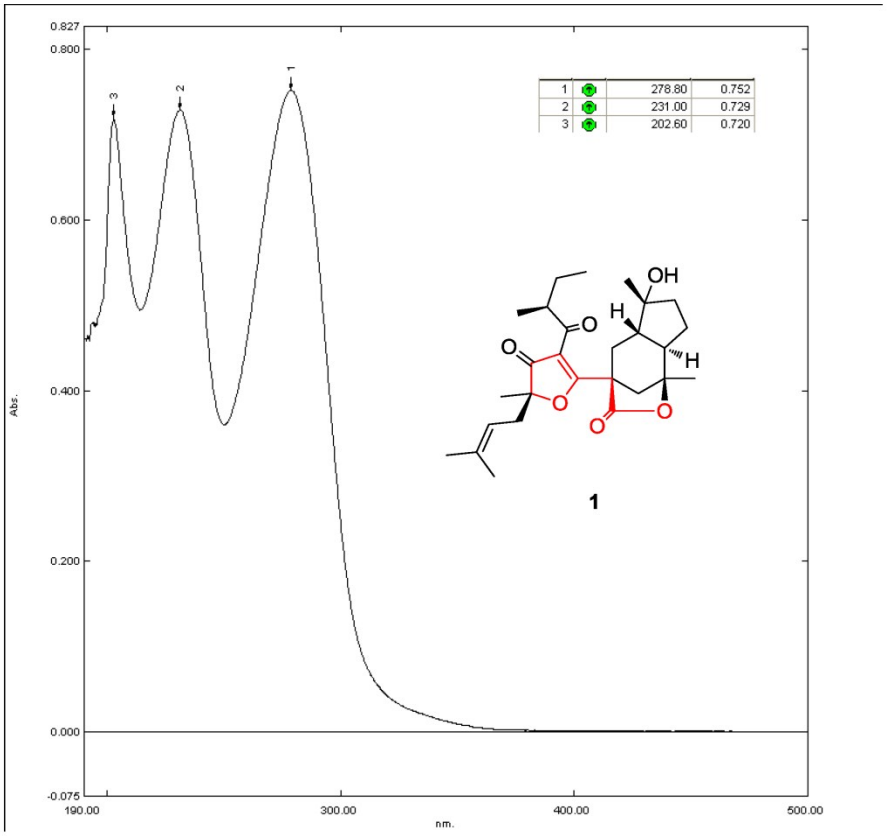

Figure S3-8. UV spectrum of furanmonogone A (**1**) in MeOH

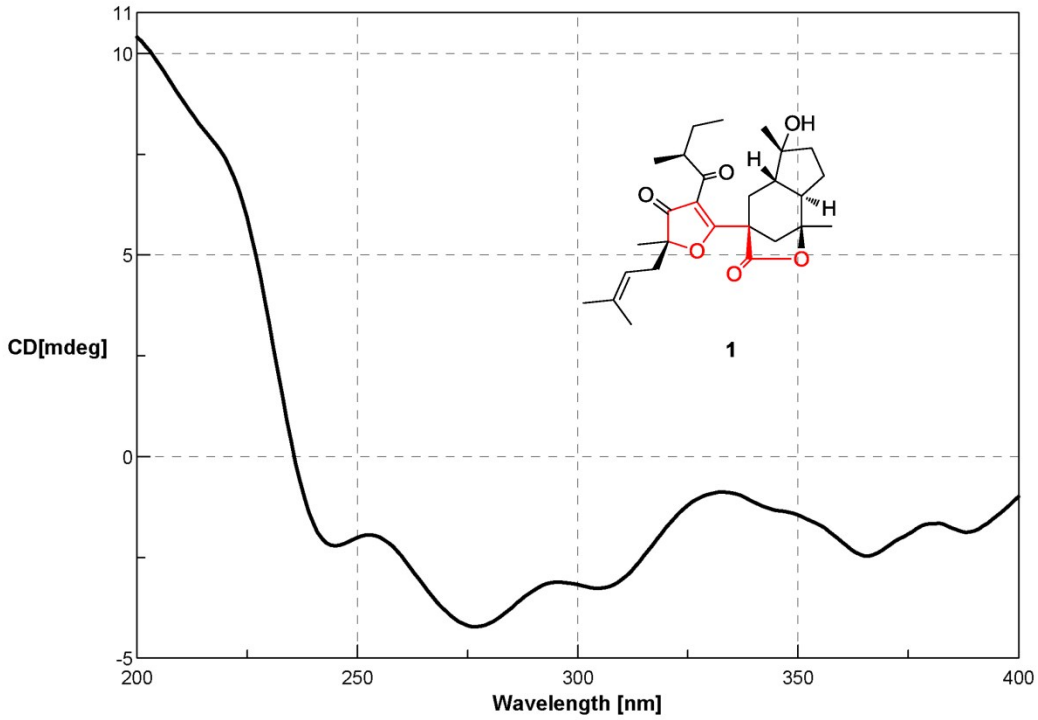

Figure S3-9. ECD spectrum of furanmonogone A (**1**) in MeOH

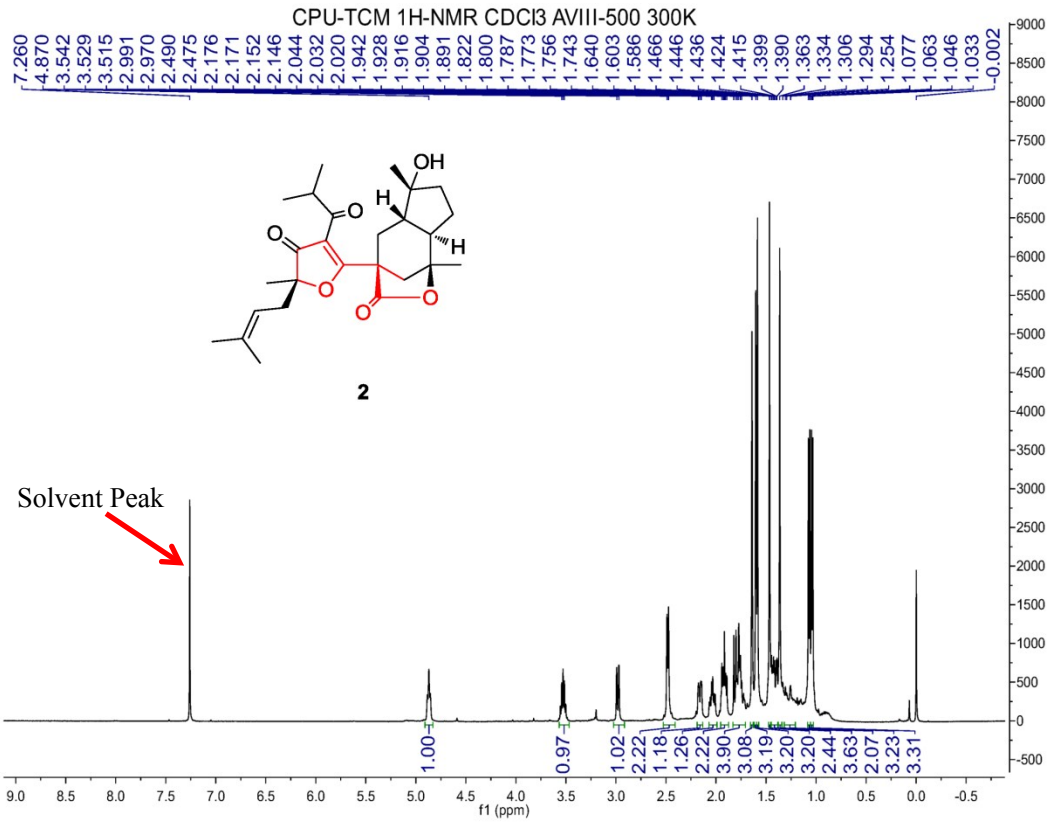

Figure S4-1. ^{1}H NMR spectrum of furanmonogone B (**2**) in $CDCl_3$

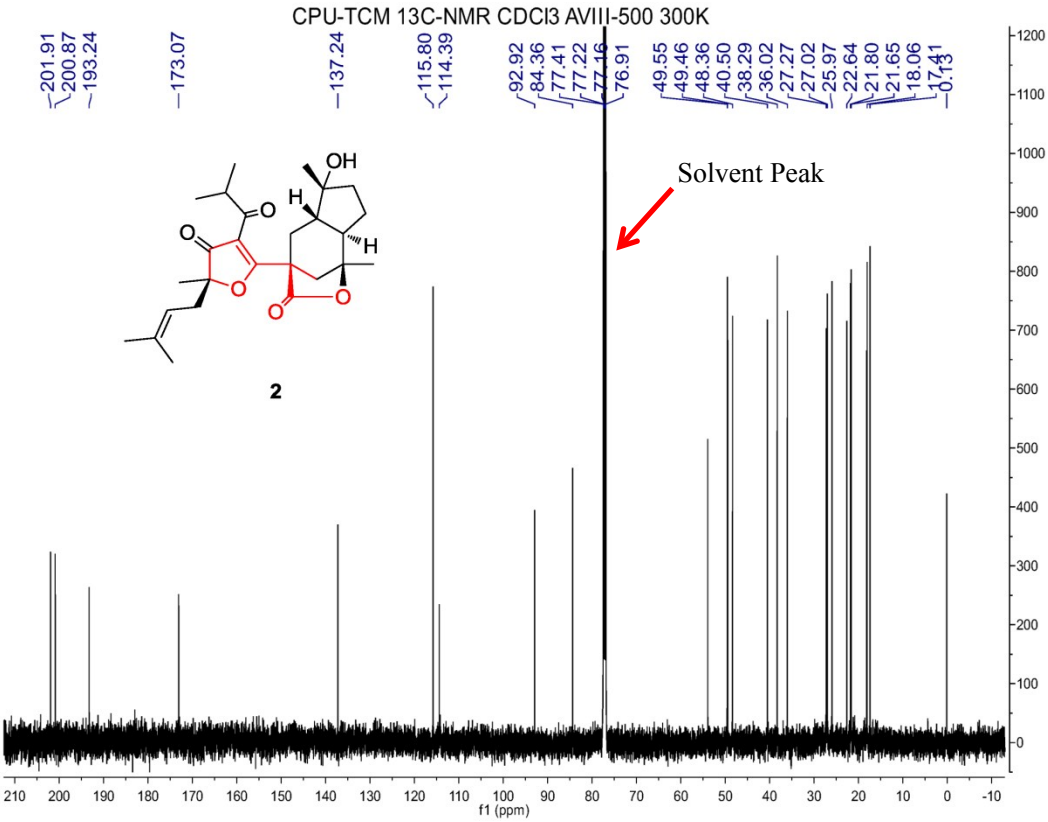

Figure S4-2. ^{13}C NMR spectrum of furanmonogone B (**2**) in $CDCl_3$

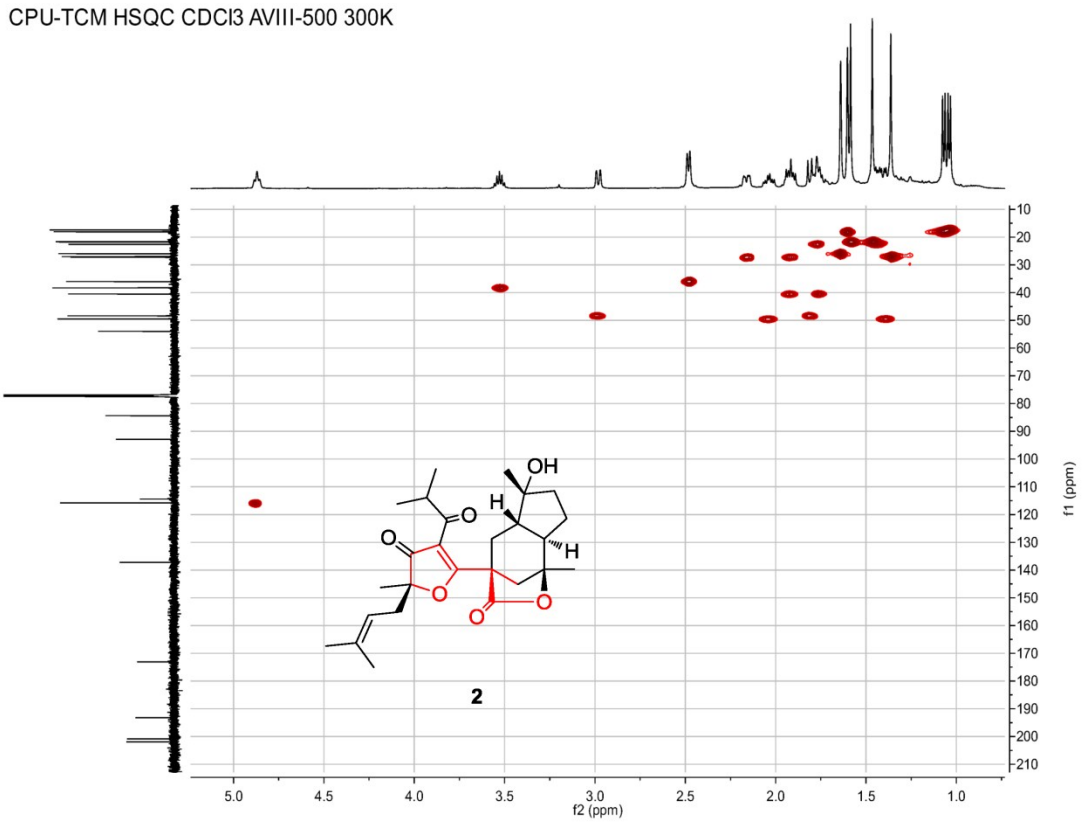

Figure S4-3. HSQC spectrum of furanmonogone B (**2**) in $CDCl_3$

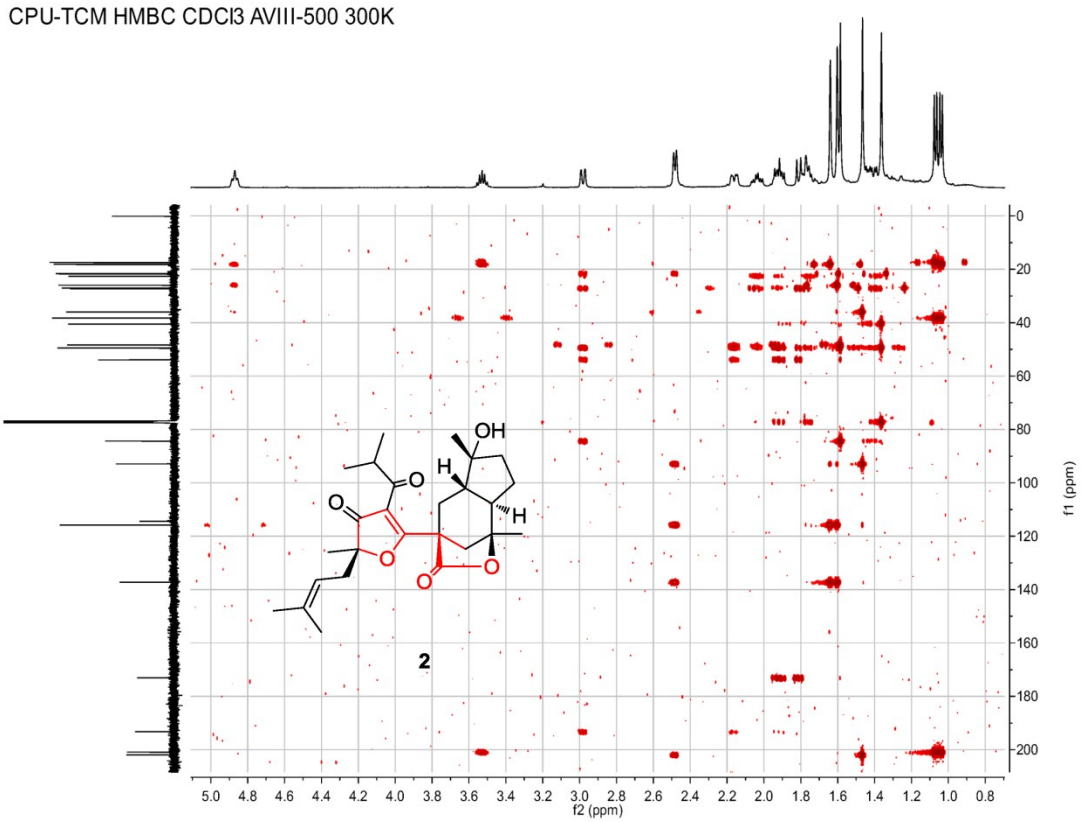

Figure S4-4. HMBC spectrum of furanmonogone B (**2**) in $CDCl_3$

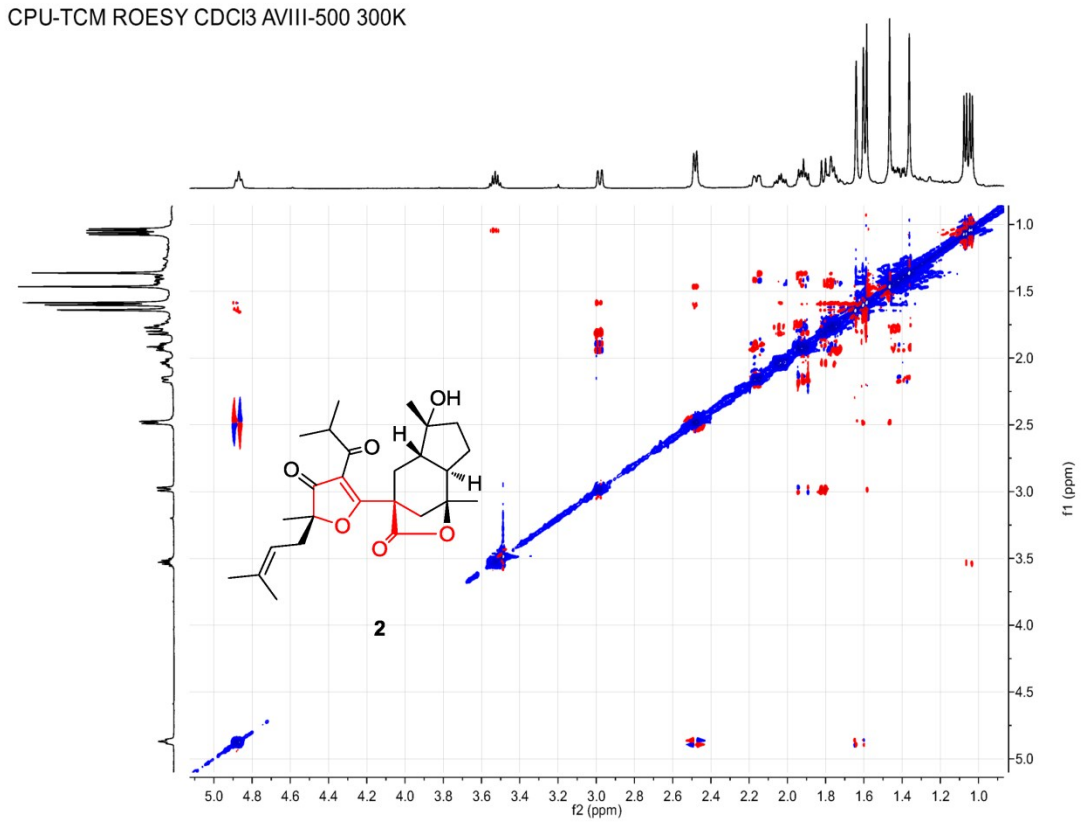

Figure S4-5. ROESY spectrum of furanmonogone B (**2**) in $CDCl_3$

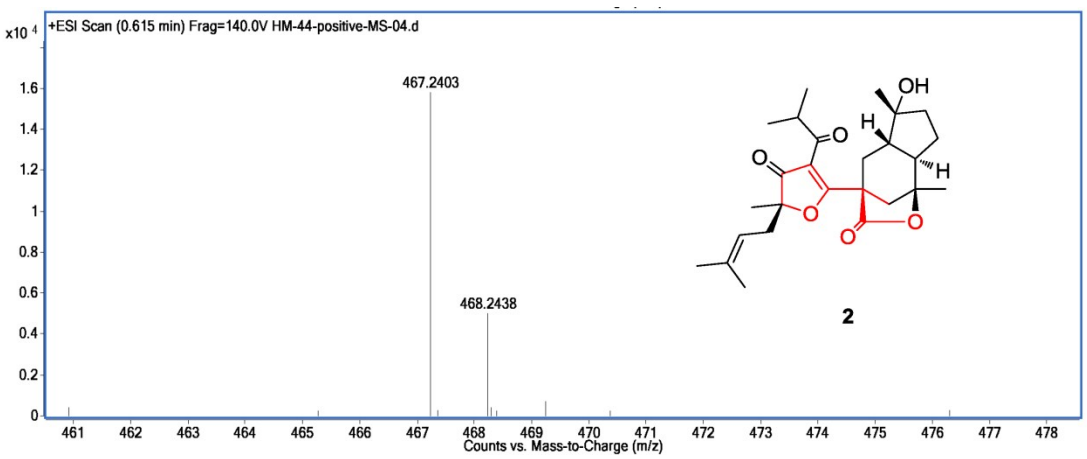

Elemental Composition Calculator

Target m/z:	467.2403	**Result type:**	Positive ions	**Species:**	$[M+Na]^+$
Elements:		C (0-80); H (0-120); O (0-30); N(0-10); Na (0-5); S (0-5)			
Ion Formula		**Calculated m/z**		**PPM Error**	
C26H36NaO6		467.2404		0.1	

Figure S4-6. HRESIMS spectrum of furanmonogone B (**2**)

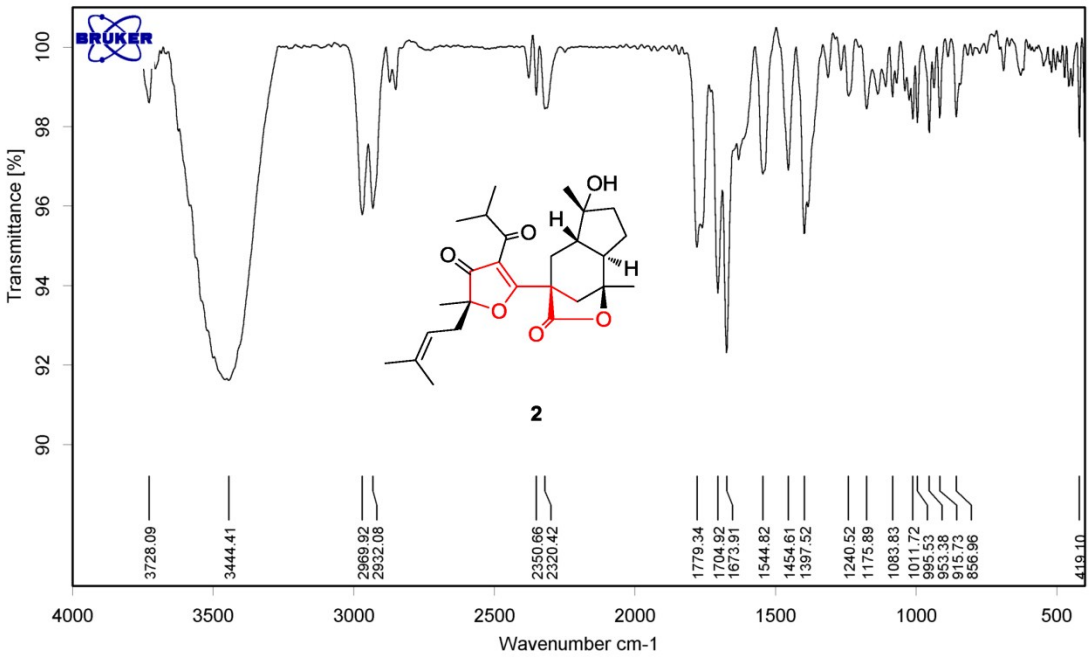

Figure S4-7. IR (KBr disc) spectrum of furanmonogone B (**2**)

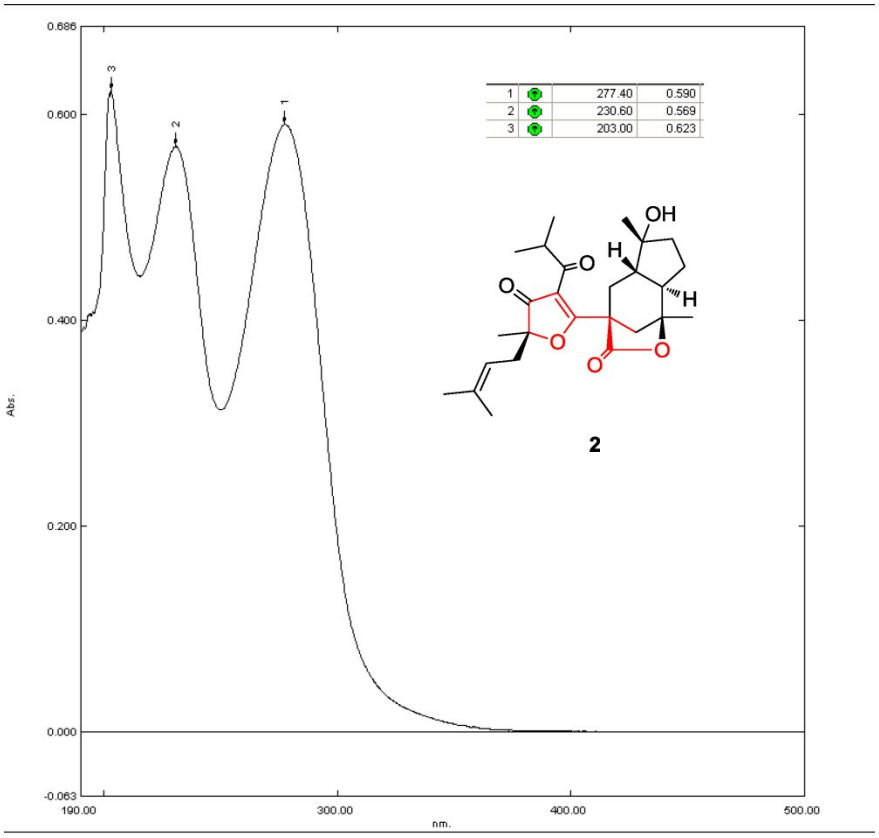

Figure S4-8. UV spectrum of furanmonogone B (**2**) in MeOH

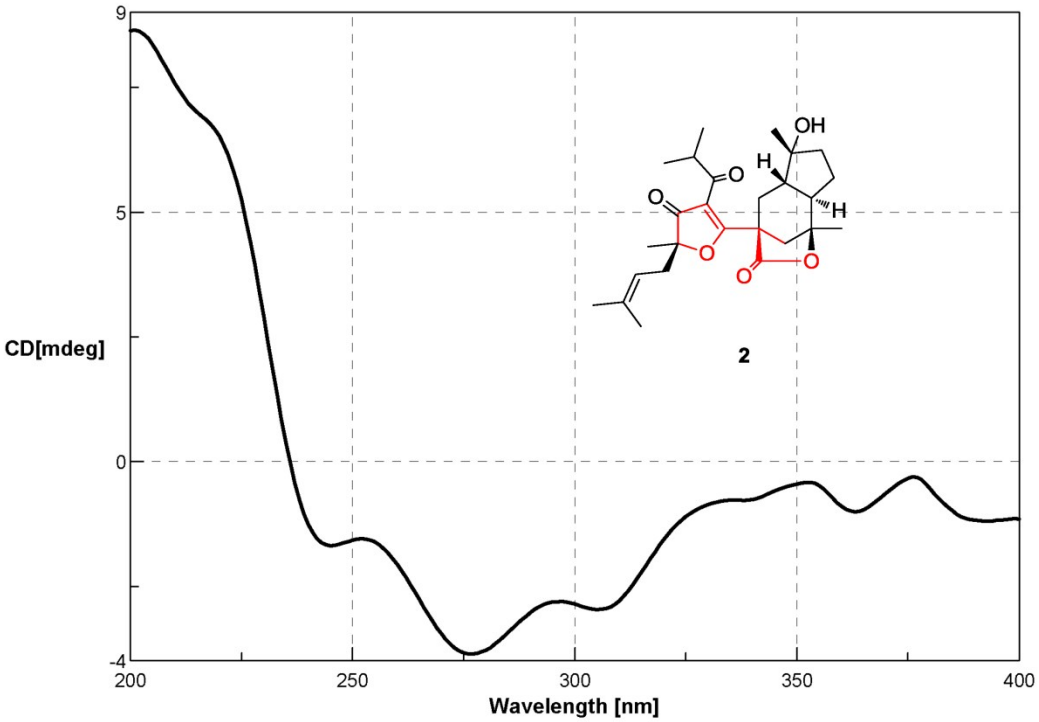

Figure S4-9. ECD spectrum of furanmonogone B (**2**) in MeOH